Velocity-comb modulation transfer spectroscopy

Xiaolei Guan,[1] Zheng Xiao,[1] Zijie Liu,[1] Zhiyang Wang,[1] Jia Zhang,[1] Xun Gao,[1] Pengyuan Chang,[2] Tiantian Shi,[3,*] and Jingbiao Chen[1,4,5]

[1] *State Key Laboratory of Photonics and Communications, Institute of Quantum Electronics, School of Electronics, Peking University, Beijing 100871, China*

[2] *Institute of Quantum Information and Technology, Nanjing University of Posts and Telecommunications, Nanjing 210003, China*

[3] *National Key Laboratory of Advanced Micro and Nano Manufacture Technology, School of Integrated Circuits, Peking University, Beijing 100871, China*

[4] *Hefei National Laboratory, Hefei 230088, China*

[5] *Peking University Handan Innovation Institute, Handan 056107, China*

(Received 12 May 2025; revised 14 October 2025; accepted 17 November 2025; published 4 December 2025)

Sub-Doppler laser spectroscopy is crucial for laser-frequency stabilization, playing a significant role in atomic physics and precision measurement. However, despite decades of development, inefficient atomic utilization remains a widespread issue. Most existing methods rely on single-frequency lasers, and due to the Doppler effect, only a small fraction (<1%) of atoms with near-zero longitudinal velocities are utilized, severely limiting improvements in the spectral signal-to-noise ratio (S/N). Here, we propose a velocity-comb modulation transfer spectroscopy (VC-MTS) solution that leverages the velocity-selective resonance of modulated N-frequency lasers, seeming as an optical comb, to enhance the utilization of nonzero-velocity atoms, which optimizes the spectral amplitude and frequency instability by N and $\sqrt{N}$ times, respectively. Unlike traditional MTS, in this work, each pair of counterpropagating lasers interacts with atoms from different longitudinal velocity groups, independently contributing to the amplitude and S/N. Preliminary proof-of-principle results show that the frequency stability of the triple-frequency laser is improved by $\sqrt{3}$ times compared to the single-frequency laser. With more frequency components, VC-MTS stabilized lasers are expected to achieve order-of-magnitude breakthroughs in frequency stability, taking an essential step toward next-generation compact optical clocks. This method also applies to quantum systems with wide velocity distributions, offering an innovative perspective on laser spectroscopy and inspiring further intriguing applications.

DOI: 10.1103/rwzv-p2fj

I. INTRODUCTION

Laser spectroscopy [1] has been one of the most active fundamental research fields in optics since the advent of lasers. As a vital tool for exploring matter-light interactions, it plays an indispensable role in investigating the spectral properties of atoms, molecules, and condensed matter. In 1971, Schawlow *et al.* proposed the saturated absorption spectroscopy (SAS) method [2], which successfully eliminated the spectral broadening induced by the Doppler effect [3–6]. Since then, sub-Doppler laser spectroscopy has advanced rapidly, driving the development of various high-resolution spectroscopic techniques, including polarization spectroscopy (PS) [7,8], two-photon spectroscopy (TPS) [9–11], and modulation transfer spectroscopy (MTS) [12–16]. These techniques are now widely applied in laser-frequency stabilization [13,17], precision measurement [18–20], and chemical analysis [21].

Among the aforementioned types of sub-Doppler laser spectroscopy, MTS is noted for its insensitivity to background absorption and suppression of low-frequency noise. Currently, the MTS-based iodine molecular clock exhibits excellent performance, achieving frequency stability on the order of 10^{-15} with good reproducibility [13,22,23], making it a recommended wavelength standard. Meanwhile, the compact MTS-based alkali metal atomic clock has also made remarkable progress, with frequency stability reaching the 10^{-14} level [17,24–26]. However, the existing configuration, in which single-frequency probe and pump beams propagate in opposite directions through the vapor cell, allows only a very small fraction of atoms (or molecules) with near-zero longitudinal velocities (along the laser propagation direction) to participate

*Contact author: tts@pku.edu.cn

Published by the American Physical Society under the terms of the Creative Commons Attribution 4.0 International license. Further distribution of this work must maintain attribution to the author(s) and the published article's title, journal citation, and DOI.

in the transition. The effective utilization of atoms is extremely low (<1%), posing significant challenges to further improving the signal-to-noise ratio (S/N, proportional to the square root of the number of effectively utilized atoms) of the spectrum. According to the Allan deviation formula $\sigma_y(\tau) = (1/K)[\Delta\nu/(\nu_0 S/N\sqrt{\tau})]$, the S/N is one of the key factors determining laser-frequency stability. Therefore, enhancing atomic utilization could open an alternative avenue for advancing MTS stabilization and other sub-Doppler laser spectroscopy-based stabilization techniques (in addition to TPS).

In 2022, Shang *et al.* [27] proposed the concept of "velocity-grating" atom interferometry and performed theoretical studies with a thermal calcium beam. The results indicated that this method is expected to enhance the amplitude of optical Ramsey fringes by a factor of 1000. In 2025, Tobias *et al.* [28] experimentally verified the feasibility of this method in a laser-cooled ^{40}Ca beam optical clock, reporting Allan deviations of $(31.4, 16.5, 3.4) \times 10^{-15}/\sqrt{\tau}$ for single-frequency, triple-frequency, and multifrequency spectroscopy, respectively. These findings highlight the significant advantages of enhancing atomic utilization in atomic-beam systems. However, in more easily integrable thermal vapor-cell MTS systems, the concept of enhancing atomic utilization has yet to be established and experimentally realized.

In this work, we propose a velocity-comb MTS (VC-MTS) frequency-stabilization scheme that enhances atomic utilization in a thermal vapor cell by leveraging the velocity-selective resonance effect of multifrequency lasers. The multifrequency components with equal frequency intervals, generated by external phase modulation of a single-frequency laser operating at 780 nm, exhibit a "frequency-fork"-like spectral profile. When applied to the atomic vapor cell in the MTS configuration, each pair of counterpropagating probe and pump lasers interacts with rubidium (Rb) atoms from different longitudinal velocity groups, which correspond one to one with the frequency components and independently contribute to the spectral amplitude and S/N. Since these atoms exhibit a mini-comb-like distribution in the longitudinal velocity domain, we refer to the resulting high-resolution spectrum as "velocity-comb" MTS. Specifically, using a triple-frequency laser as an example, we achieve an improvement in laser frequency stability from $7.5 \times 10^{-12}/\sqrt{\tau}$ to $4.3 \times 10^{-12}/\sqrt{\tau}$ (for τ from 1 s to 10 s). This result preliminarily validates the effectiveness of our scheme.

In the future, this scheme can also be extended to any quantum system with a wide velocity distribution, showing great potential in the realization of 10^{-16}-level iodine molecular optical frequency standards [13,23], as well as offering another pathway to improve the S/N of some other molecular frequency standards (such as CHF_3 [29], CH_4 [30,31], and CO_2 [32]). Of note, it could serve as an innovative, versatile, and high-performance technique for existing sub-Doppler laser spectroscopy, with the potential to drive further advancements in fields such as quantum precision measurement, space science, metrology, and timekeeping.

II. EXPERIMENTAL PRINCIPLE

Figure 1(a) illustrates the schematic of the VC-MTS. A homemade 780-nm narrow-linewidth diode laser (60 kHz linewidth in free-running mode, reduced to 10 kHz after locking) with single-frequency output is phase modulated by an electro-optic modulator (EOM1) with a resonance frequency of 50 MHz, generating multiple sidebands in addition to the main frequency (details of the experimental setup are available in the Appendix). Focusing on the ±1st-order sidebands as a representative case, we analyze the spectral amplitude enhancement principle based on the ^{87}Rb $5^2S_{1/2}$ $F = 2 \rightarrow 5^2P_{3/2}$ $F' = 3$ transition.

As shown in Fig. 1(a), ν_{23} represents the frequency of the $F = 2 \rightarrow F' = 3$ transition. $\nu_{+1} = \nu_{23} + \Delta$ and $\nu_{-1} = \nu_{23} - \Delta$ represent the frequencies of the +1- and −1-order sidebands generated by EOM1 modulation, respectively, where $\Delta = 50$ MHz is the modulation frequency of EOM1. When the laser frequency is scanned to the $F = 2 \rightarrow F' = 3$ transition, the three frequency components, ν_{23}, ν_{+1}, and ν_{-1}, simultaneously interact with the atomic medium as both probe and pump beams. Among these, the ν_{23} component only interacts with atoms with near-zero longitudinal velocity. For atoms with certain nonzero velocities, such as those in the $+\upsilon$ velocity group that satisfy the Doppler condition $\nu_{-1} + \vec{k}_1 \cdot \vec{\upsilon} = \nu_{23}$, the pump beam from the ν_{-1} component [Pump2, see the inset of Fig. 1(a)] excites the $F = 2 \rightarrow F' = 3$ transition, where $\vec{k}_1$ is the wave vector of the Pump2 laser. Similarly, the $+\upsilon$ velocity group also satisfies the Doppler condition $\nu_{+1} - \vec{k}_2 \cdot \vec{\upsilon} = \nu_{23}$, allowing the probe beam from the ν_{+1} component (Probe1) to excite the $F = 2 \rightarrow F' = 3$ transition, with $\vec{k}_2$ as the wave vector of the Probe1 laser. Both Pump2 and Probe1 interact with atoms in the $+\upsilon$ velocity group, thereby enhancing the spectral amplitude of the $F = 2 \rightarrow F' = 3$ transition. For the same reason, Pump1 and Probe2 can excite atoms in the $-\upsilon$ velocity group to participate in the $F = 2 \rightarrow F' = 3$ transition. Additionally, minor contributions arise from the weaker ±2nd-order sidebands ($\Delta' = 100$ MHz) and ±3rd-order sidebands ($\Delta'' = 150$ MHz), which are not shown in the bottom of Fig. 1(a). These atoms excited by the multifrequency components form a mini-comb-like distribution in the longitudinal velocity domain, ultimately resulting in an accumulated enhancement in the amplitude of the VC-SAS and VC-MTS.

The spectra before and after modulation by EOM1 are measured using a spectrum analyzer, with the ordinate

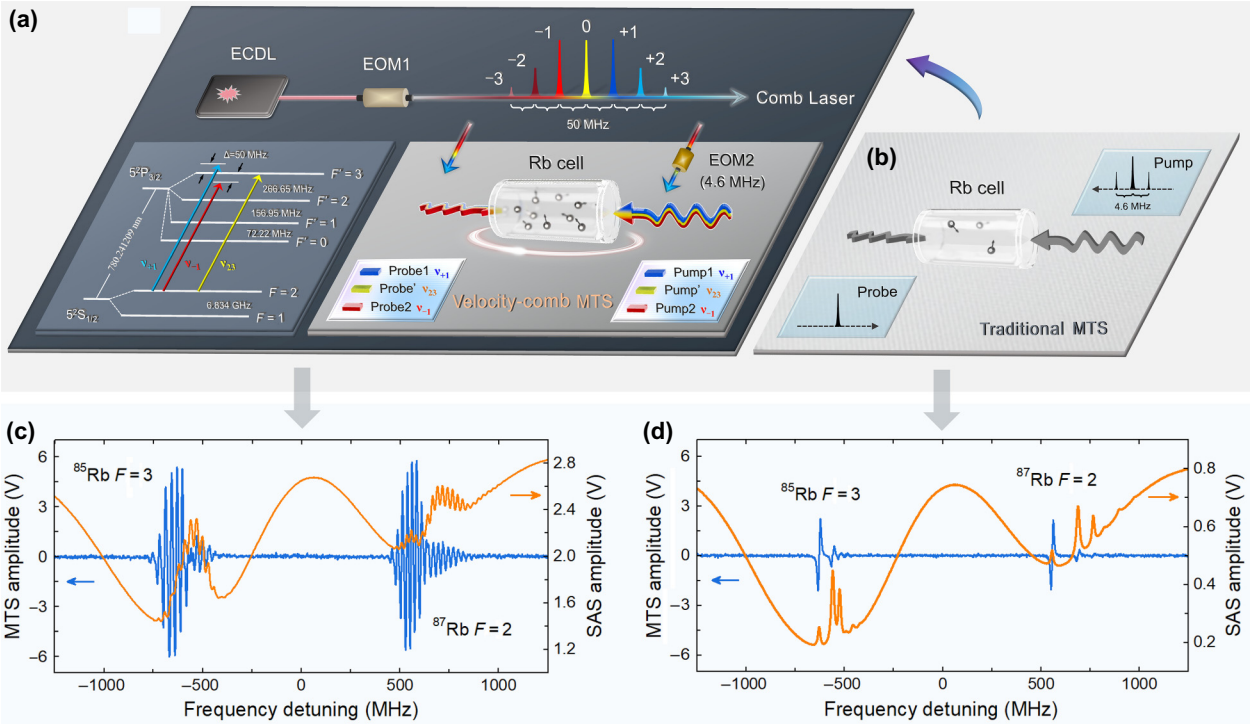


FIG. 1. Conceptual illustration of the velocity-comb MTS. (a) Interaction process of nonzero velocity atoms with multifrequency lasers. EOM, electro-optic modulator. The yellow component (ν_{23}) represents the frequency of the $F = 2 \rightarrow F' = 3$ transition, while the blue (ν_{+1}) and red (ν_{-1}) components correspond to the frequencies of the $+1$ and -1 order sidebands generated by modulation, respectively. The modulation frequency (Δ) of the EOM1 is 50 MHz. In the thermal Rb vapor cell, atoms with various velocity groups are present, and their overall velocity distribution follows the Maxwell-Boltzmann distribution. (b) Traditional MTS utilizes single-frequency lasers to interact with atoms. In (a),(b), the pump beam is also phase modulated at 4.6 MHz for modulation transfer. (c),(d) Comparison of the SAS signal (orange curve) and MTS signal (blue curve) for the triple-frequency and single-frequency lasers. The left and right sides correspond to the ^{85}Rb $5^2S_{1/2}$ $F = 3$ and ^{87}Rb $5^2S_{1/2}$ $F = 2$ to $5^2P_{3/2}$ transitions, respectively.

scale being linear in intensity. According to the characteristics of the Bessel function, within a certain modulation depth, the sideband intensity of EOM1 phase modulation decreases significantly with increasing order. Therefore, we select an appropriate modulation amplitude to make the intensity of the $\pm$1st-order sidebands comparable to the main frequency, while the $\pm$2nd- and $\pm$3rd-order sidebands play a weaker role. When the single-frequency intensity is consistent with the triple-frequency (0 and $\pm$1st-order) intensities, we measure the SAS and MTS signals for both lasers and present the results in Fig. 1(c) and 1(d). The left and right sides correspond to the ^{85}Rb $5^2S_{1/2}$ $F = 3$ and ^{87}Rb $5^2S_{1/2}$ $F = 2$ to $5^2P_{3/2}$ transitions, respectively. It is evident that the SAS and MTS signals of the triple-frequency laser exhibit a multipeak structure with increased atomic interactions, and the amplitude is significantly enhanced compared to that of the single-frequency laser. To quantitatively demonstrate the enhancement of the spectral signal, we then measure the VC-SAS and VC-MTS under different numbers of frequency components and calibrate the MTS amplitude of the ^{87}Rb $5^2S_{1/2}$ $F = 2 \rightarrow 5^2P_{3/2}$ $F' = 3$ cycling transition.

III. RESULTS

A. Relationship between frequency components and MTS amplitude

The number of frequency components can be controlled by adjusting the modulation amplitude of EOM1 [see the upper parts of Figs. 2(a)–2(e)], but the peak intensity of the main components needs to be kept equal. When the laser is unmodulated, it has only one frequency component, resulting in the traditional single-frequency spectrum shown in Fig. 2(a), with a corresponding MTS amplitude of 4.1 V. When the modulation amplitude is 15 dBm, two small 1st-order sidebands appear on either side of the main frequency. Although their intensities are relatively weak, we can still distinguish the multifrequency effect and the increase in MTS amplitude from Fig. 2(b). When the modulation amplitude is 20 dBm, the $\pm$1st-order sidebands become more prominent, and the enhancement of the VC-SAS and VC-MTS can be clearly seen in Fig. 2(c), with a corresponding MTS amplitude of 8.8 V. Further increasing the modulation amplitude to 22 dBm equalizes the intensities of the $\pm$1st-order sidebands with the

main frequency, producing a triple-frequency spectrum as shown in Fig. 2(d). The multipeak structure is more pronounced, and the MTS amplitude reaches 11.9 V. When the modulation amplitude is further increased to 25 dBm, the enhanced sidebands begin suppressing the main frequency, and the ±1st-order sidebands dominate the contribution. Comparing Figs. 2(d) and 2(e), the amplitude of the triple-frequency spectrum is obviously higher than that of the dual-frequency spectrum, with the corresponding dual-frequency MTS signal at 10.4 V. From these results, we can infer that the enhancement of spectral amplitude is positively correlated with the number of laser-frequency components. Notably, each frequency component requires a certain power allocation. In this work, the total MTS powers corresponding to the five cases of unmodulated, 15, 20, 22, and 25 dBm are 0.17, 0.2, 0.28, 0.61, and 0.36 mW, respectively.

B. Characterization of velocity-comb MTS

Under the modulation amplitude of 22 dBm, we further investigate the working characteristics of the VC-MTS. The probe beam has a diameter of 2 mm, corresponding to an atomic transit time of approximately 8 μs, which is much longer than the modulation period of 20 ns. To quantitatively evaluate the system performance, we introduce the MTS slope as a key characterization parameter. A larger slope indicates a higher S/N of the spectrum and greater sensitivity to frequency fluctuations. In our experiment, the MTS slope is calculated by dividing the peak-to-peak amplitude of the signal by the linewidth between the two peaks. The calibration method for amplitude and linewidth is illustrated in Fig. 3(a), where the known frequency interval of 133.3 MHz between the $F = 2 \rightarrow F' = 3$ transition peak and the $F = 2 \rightarrow F' = 2, 3$ crossover peak in the SAS is used as a frequency reference. Figure 3(b) shows the relationship between the MTS slope and the pump laser power, corresponding to the ^{87}Rb $5^2S_{1/2}$ $F = 2 \rightarrow 5^2P_{3/2}$ $F' = 3$ cycling transition (same below). The red circles, orange triangles, and blue diamonds represent measurements taken at probe laser powers of 0.05, 0.1, and 0.15 mW, respectively. As the pump power increases, all three curves exhibit an initial increase followed by a decrease. This behavior results from the competition between the enhanced modulation transfer efficiency and the effects of power broadening and saturation. At low pump powers, increasing the pump intensity promotes stronger atomic excitation and deeper spectral hole burning, thereby producing a higher MTS signal after modulation transfer. However, when the pump power exceeds a certain threshold, power broadening significantly increases the linewidth, while the saturation effect limits further growth of the signal amplitude, leading to a gradual decrease in the MTS slope. The experimental results indicate that the MTS slope reaches its maximum at a pump power of approximately 0.4 mW.

Figure 3(c) illustrates the dependence of the MTS slope on the probe laser power at a fixed pump power of 0.4 mW. At low probe powers, increasing the probe intensity significantly enhances the interaction between the probe beam and the atoms, resulting in a rapid increase in the MTS slope. However, as the probe power continues to rise, power broadening induced by the probe itself becomes increasingly pronounced. The associated linewidth broadening counteracts the gain in signal amplitude, causing the MTS slope to approach saturation at around 0.15 mW. Furthermore, the temperature of the Rb cell also exerts a notable influence on the MTS slope [see Fig. 3(d)]. At relatively low temperatures, heating the cell increases the atomic density, thereby enhancing the signal amplitude and increasing the MTS slope. However, once the temperature exceeds a certain value (around 50 °C in our experiment), intensified thermal motion of atoms results in pronounced collisional broadening, leading to a noticeable increase in the spectral linewidth. Meanwhile, the strengthened resonant absorption of the unmodulated probe beam further weakens the effective modulation transfer signal, ultimately limiting the continued growth of the MTS slope.

C. Verification of frequency stability improvement

Next, we experimentally verify the improvement in frequency stability achieved with the VC-MTS scheme. The saturated absorption signal and the spectral S/N of a single-frequency laser follow the expressions:

$$P_S(\omega) = P\left[1 - \kappa \frac{(\Gamma/2)^2}{(\omega - \omega_0)^2 + (\Gamma/2)^2}\right] \tag{1}$$

and

$$\frac{S}{N}_{(S)} = \kappa\sqrt{\frac{P\tau}{\hbar\omega}}, \tag{2}$$

where ω is the laser frequency, P is the laser power, κ is the dimensionless saturation parameter, ω_0 is the center frequency of the atomic transition, Γ is the homogeneous linewidth, and τ is the integration time. When a multifrequency comb laser is applied to the atoms, each pair of oppositely directed pump and probe lasers can interact with atoms from different longitudinal velocity groups and independently contribute to the absorption coefficient. Thus, the saturated absorption signal of the multifrequency laser can be expressed as

$$P_M(\omega) = \sum_n P_n\left[1 - \kappa_n \frac{(\Gamma/2)^2}{(\omega - \omega_0)^2 + (\Gamma/2)^2}\right]. \tag{3}$$

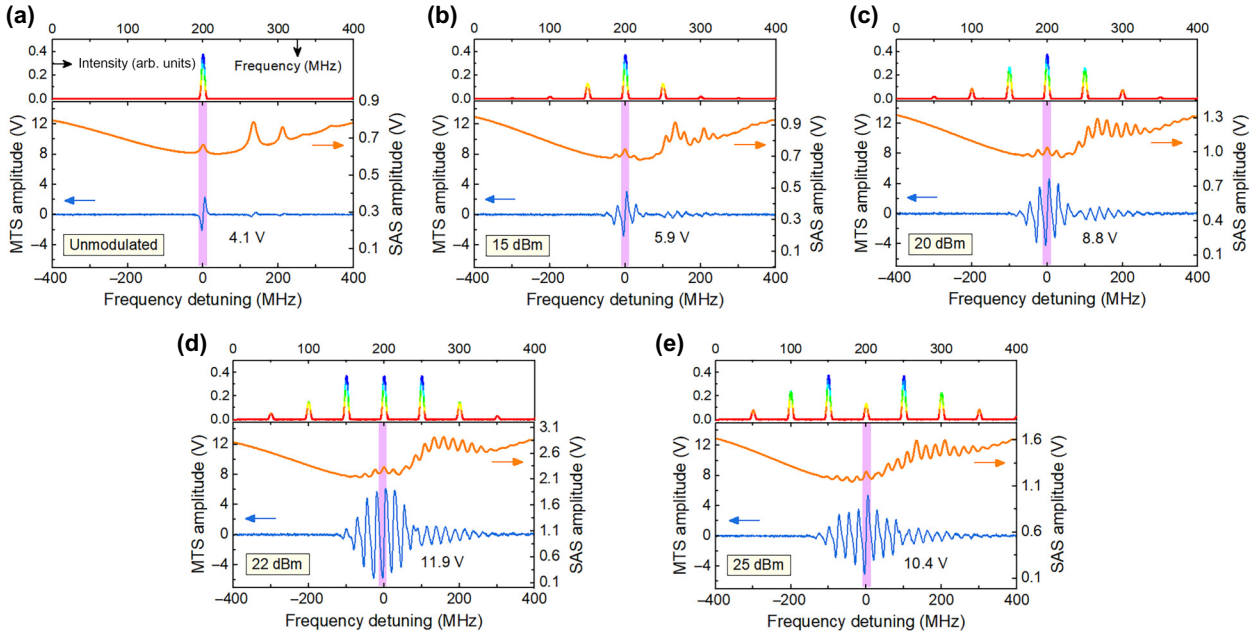


FIG. 2. Velocity-comb atomic spectroscopy under different frequency components (orange curve: SAS, blue curve: MTS). From (a) to (e), the modulation amplitudes of EOM1 are as follows: unmodulated, 15, 20, 22, and 25 dBm, respectively. The purple-shaded region corresponds to the ^{87}Rb $5^2S_{1/2}$ $F = 2 \rightarrow 5^2P_{3/2}$ $F' = 3$ cycling transition. The upper part of each subplot displays the laser spectrum at different modulation amplitudes. Here, the center frequency of 200 MHz represents the frequency shift before heterodyne measurements.

For N frequency components, the spectral S/N is then deduced as

$$\frac{S}{N}_{(M)} = \kappa\sqrt{\frac{NP\tau}{\hbar\omega}}, \tag{4}$$

which is improved by a factor of $\sqrt{N}$ compared to the single-frequency spectrum.

Stabilizing the frequency of the 780-nm diode laser to the $F = 2 \rightarrow F' = 3$ cycling transition of the single-frequency spectrum shown in Fig. 2(a) and the triple-frequency spectrum shown in Fig. 2(d), respectively, and performing beat measurements with a 780-nm ultrastable reference laser (which is also locked to the $F = 2 \rightarrow F' = 3$ transition and frequency shifted by a 200-MHz acousto-optic modulator to introduce an offset), we obtain the frequency stability comparison results shown in Fig. 3(e). The 780-nm ultrastable reference laser exhibits known high frequency stability [black triangles in Fig. 3(e)], in comparison with an optical comb referenced to a hydrogen clock [green stars in Fig. 3(e)]. As shown in the results, over an averaging time of 10 s, the Allan deviations of the single-frequency and triple-frequency lasers are $7.5 \times 10^{-12}/\sqrt{\tau}$ and $4.3 \times 10^{-12}/\sqrt{\tau}$, respectively. Across the entire averaging time measurement range, the frequency stability of the triple-frequency laser is improved by nearly $\sqrt{3}$ times compared to the single-frequency laser. This result is in good agreement with the theoretical expectation. As a preliminary proof-of-principle, the optical path is currently dispersed on the optical table, without active control of environmental factors such as temperature and mechanical vibrations. Therefore, the system's frequency stability is limited to the 10^{-12} level. Upon validation of this scheme, we will integrate the system with anti-interference measures and optimize residual amplitude modulation (RAM) [33–35], power stability [36], etc., aiming to further improve the frequency stability based on the best-performing thermal vapor-cell rubidium optical frequency standard [17]. In addition, we find that by locking the laser frequency to the zero-crossing points of different dispersion curves in the VC-MTS, various stabilized lasers close to the atomic transition frequency can be easily achieved, which is an additional advantage of this scheme.

D. Prediction for E-15 stability lasers referenced to thermal Rb atoms

Among alkali metals, Rb stands out for its low melting point, high abundance, and ease of extraction. A thermal atomic vapor cell heated above room temperature can produce sufficient saturated vapor pressure, making Rb an attractive quantum reference ensemble for low-cost and miniaturized optical clocks. Over decades of technological advancement, MTS stabilization based on Rb atoms has commonly achieved laser-frequency stabilities on the order of 10^{-14} [17,24,25]. Following the approach proposed in this work, we estimate that the frequency stability

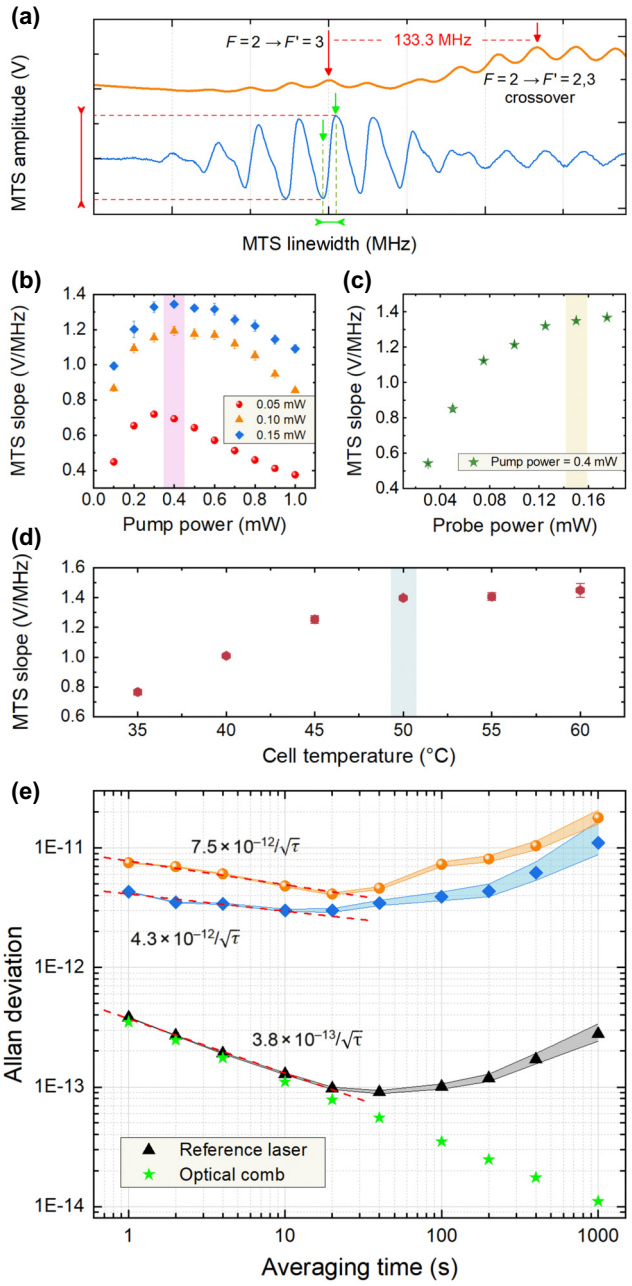


FIG. 3. Working characteristics of the velocity-comb MTS. (a) Calibration of the VC-MTS linewidth and amplitude. The slope of the VC-MTS as a function of (b) pump laser power, (c) probe laser power, and (d) cell temperature. The red circles, orange triangles, and blue diamonds in (b) correspond to probe laser powers of 0.05, 0.1, and 0.15 mW, respectively. All values are measured for the ^{87}Rb $5^2S_{1/2}$ $F = 2 \rightarrow 5^2P_{3/2}$ $F' = 3$ cycling transition. (e) Allan deviations of the single-frequency laser (orange circles) and the triple-frequency laser (blue diamonds) stabilized by MTS. The data are derived from heterodyne beat measurements with a 780-nm ultrastable reference laser (black triangles), whose frequency stability is evaluated by beating it with an optical comb (green stars) referenced to a hydrogen clock. The shaded areas denote the error bands. The red dashed lines represent the linear fit to the short-term data points.

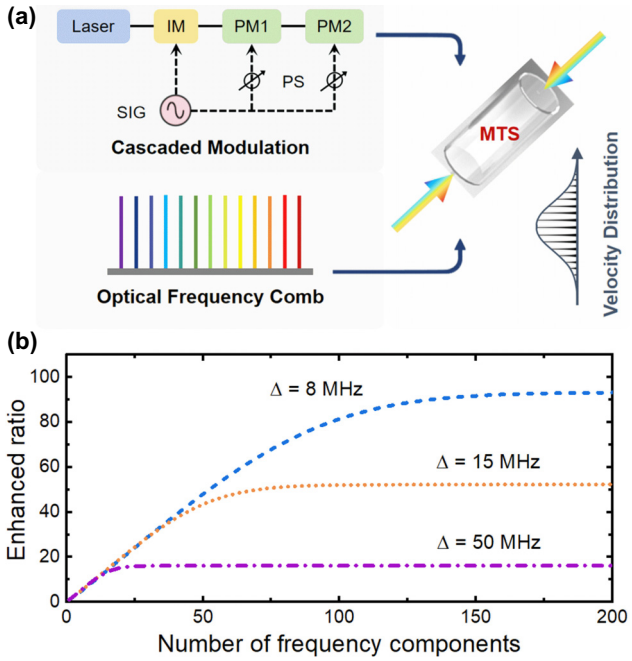


FIG. 4. Prospects of velocity-comb MTS. (a) Increased frequency components for VC-MTS stabilization using cascaded modulation or an optical frequency comb. IM, intensity modulator; PM, phase modulator; SIG, signal generator; PS, phase shifter. (b) Amplitude enhancement ratio of the velocity-comb atomic spectroscopy as a function of the number of frequency components (N) for different frequency intervals (Δ).

of an Rb 780-nm laser could potentially reach the 10^{-15} level. The specific scheme is illustrated in Fig. 4(a).

Using cascaded modulation [37,38] or an optical frequency-comb [39] to generate multiple frequency comb components and applying them to the MTS stabilization system, we theoretically calculate the amplitude enhancement ratio of the velocity-comb atomic spectroscopy under different frequency intervals ($\Delta = 8$, 15, and 50 MHz) and numbers of frequency components (N). The ratio is simply given by

$$\mathcal{R} \propto \frac{\sum_n (e^{-\alpha_n' l} - e^{-\alpha_0' l})}{e^{-\alpha l} - e^{-\alpha_0 l}}, \tag{5}$$

where α and α_0 represent the absorption coefficients of the probe laser in the single-frequency case, with and without the pump laser, respectively; α_n' and α_0' represent the absorption coefficients of the probe laser corresponding to the nth frequency in the multifrequency comb case, with and without the pump laser, respectively; l is the length of the Rb cell. As shown in Fig. 4(b), for a fixed Δ, the enhancement ratio initially increases linearly with N but gradually saturates once the total spectral width exceeds the Doppler range. Smaller Δ values allow more frequency components within the Doppler range, significantly

increasing the amplitude enhancement ratio by engaging more atomic velocity groups in the transition. When $\Delta = 8$ MHz, the enhancement ratio approaches 100-fold. However, it should be noted that if Δ becomes too small, the overlap between the spectra corresponding to each frequency component and their crossover spectra may lead to pronounced linewidth broadening. In this case, even though the amplitude enhancement ratio is quite high, the overall S/N may not necessarily improve. Conversely, if Δ is too large such that the modulation period $(1/\Delta)$ is much shorter than the atomic relaxation time $(1/\Gamma)$, the atoms cannot fully respond to the rapid variations of the optical field, resulting in a slight reduction in the spectral signal amplitude. Therefore, the optimal value of Δ should be determined by balancing these factors and further verified through subsequent experimental investigations. Moreover, for the 420-nm transition ($5^2S_{1/2} \rightarrow 6^2P_{3/2}$, $\Gamma =$ 1.45 MHz), which has a narrower natural linewidth compared to the 780-nm transition ($5^2S_{1/2} \rightarrow 5^2P_{3/2}$, $\Gamma = 6.06$ MHz), we predict that it holds great potential for achieving order-of-magnitude improvement in laser frequency stability [25].

IV. CONCLUSION

In this work, we propose a VC-MTS concept and apply it to the Rb 780-nm system, preliminarily demonstrating its ability to enhance laser-frequency stability by a factor of $\sqrt{N}$. Compared to traditional MTS, this approach effectively overcomes the critical challenge of low atomic utilization that has persisted for half a century. Next, we plan to add cascaded modulation [37,38] or use optical frequency combs [39] to generate more frequency components, aiming to achieve frequency stability of 10^{-15} for the thermal vapor-cell Rb optical clock and 10^{-16} for the iodine molecular clock. Furthermore, this method is universal for any quantum system with a wide velocity distribution. It can also be incorporated into the existing technical framework as an emerging spectroscopic technique, potentially opening up broader application scenarios in quantum precision measurement [40], fundamental science [41–43], and advanced technology [44,45] through continuous advancements.

ACKNOWLEDGMENTS

This research was funded by the Innovation Program for Quantum Science and Technology (2021ZD0303200), China Postdoctoral Science Foundation (BX2021020), National Natural Science Foundation of China (NSFC) (62405007), Natural Science Foundation of Jiangsu Province (BK20240613), Fund of State Key Laboratory of Photonics and Communications, P. R. China (2025QZKF01), Hebei Provincial Natural Science Foundation Basic Research Special Project - 2025 Basic Research Program Proof-of-Concept Project (F202510 9009), and JSJL2024205XXXX.

J. Chen conceived the idea of velocity-comb modulation transfer spectroscopy by improving the atomic utilization ratio in frequency-stabilized laser systems. X. Guan performed the experiments and wrote the manuscript. X. Guan and Z. Xiao carried out the theoretical calculations. Z. Liu, Z. Wang, J. Zhang, X. Gao, P. Chang, and T. Shi participated in the discussion of results and revision of the manuscript.

The authors declare no competing interests.

DATA AVAILABILITY

The data that support the findings of this article are not publicly available upon publication because it is not technically feasible and/or the cost of preparing, depositing, and hosting the data would be prohibitive within the terms of this research project. The data are available from the authors upon reasonable request.

APPENDIX: EXPERIMENTAL DETAILS

The experimental setup of the VC-MTS system is illustrated in Fig. 5. The output of the 780-nm narrow-linewidth diode laser first passes through an isolator (ISO) to suppress back reflections. It is then split into two beams by a half-wave plate (HWP) and a polarizing beam splitter (PBS), with the transmitted beam serving as the output light and the reflected beam directed for multifrequency modulation. The EOM1, with a resonance frequency of 50 MHz mentioned above, is used to modulate the single-frequency laser into a multifrequency beam. To observe the frequency distribution of the multifrequency laser, the single-frequency laser is shifted by 200 MHz using an acousto-optic modulator (AOM) before EOM1 modulation. By combining the frequency-shifted laser with the multifrequency laser and performing heterodyne measurements, the complete spectrum is displayed on the spectrum analyzer (Keysight N9010B).

The multifrequency laser output from EOM1 then enters the MTS system for frequency stabilization. It is further divided into probe and pump beams. The pump beam is phase modulated by an electro-optic modulator (EOM2) with a resonance frequency of 4.6 MHz. After reflection, it passes through the Rb cell in reverse coincidence with the probe beam. The HWP placed before EOM2 is used to adjust the laser's polarization direction, aligning it with the main axis of the EOM2 crystal. The Rb cell is temperature-controlled and magnetically shielded to isolate it from environmental interference. After a four-wave mixing process with the pump beam in the Rb cell, the probe beam is received by a photoelectric detector (PD), which contains modulation information. The signal received by PD is filtered, amplified, and then mixed with a sine signal at the

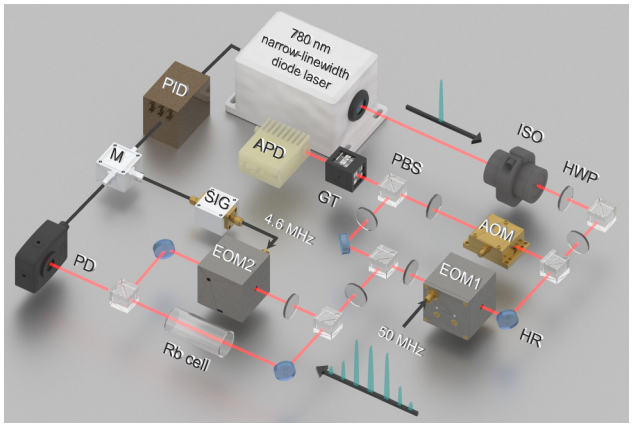


FIG. 5. Experimental setup of the velocity-comb MTS system. ISO, isolator; HWP, half-wave plate; PBS, polarizing beam splitter; HR, high-reflection mirror; EOM, electro-optic modulator; AOM, acousto-optic modulator; GT, Glan-Taylor prism; APD, avalanche photodiode; PD, photoelectric detector; SIG, signal generator; M, mixer; PID, proportion-integral-derivative locking system.

same frequency as the EOM2 driving signal. The dispersionlike signal (VC-MTS) output from the mixer serves as the error signal, which is fed back to three different frequency response ports through a proportion-integral-derivative (PID) locking system: slow PZT port, slow current port, and fast diode current port. By locking the frequency of the 780-nm diode laser to the zero-crossing point of the error signal, a stabilized laser corresponding to the hyperfine transition frequency of Rb atoms is achieved.

[1] W. Demtröder, *Laser Spectroscopy 2: Experimental Techniques* (Springer, Berlin Heidelberg, 2015).

[2] T. W. Hänsch, I. S. Shahin, and A. L. Schawlow, High-resolution saturation spectroscopy of the sodium *D* lines with a pulsed tunable dye laser, Phys. Rev. Lett. **27**, 707 (1971).

[3] T. W. Hänsch, I. S. Shahin, and A. L. Schawlow, Optical resolution of the Lamb shift in atomic hydrogen by laser saturation spectroscopy, Nat. Phys. Sci. **235**, 63 (1972).

[4] S. Haroche and F. Hartmann, Theory of saturated-absorption line shapes, Phys. Rev. A **6**, 1280 (1972).

[5] J. L. Hall, C. J. Bordé, and K. Uehara, Direct optical resolution of the recoil effect using saturated absorption spectroscopy, Phys. Rev. Lett. **37**, 1339 (1976).

[6] K. B. MacAdam, A. Steinbach, and C. Wieman, A narrow-band tunable diode laser system with grating feedback, and a saturated absorption spectrometer for Cs and Rb, Am. J. Phys. **60**, 1098 (1992).

[7] C. Wieman and T. W. Hänsch, Doppler-free laser polarization spectroscopy, Phys. Rev. Lett. **36**, 1170 (1976).

[8] T. W. Hansch and B. Couillaud, Laser frequency stabilization by polarization spectroscopy of a reflecting reference cavity, Opt. Commun. **35**, 441 (1980).

[9] A. C. Tam and C. K. N. Patel, Two-photon absorption spectra and cross-section measurements in liquids, Nature **280**, 304 (1979).

[10] D. Meshulach and Y. Silberberg, Coherent quantum control of two-photon transitions by a femtosecond laser pulse, Nature **396**, 239 (1998).

[11] Z. L. Newman, V. Maurice, C. Fredrick, T. Fortier, H. Leopardi, L. Hollberg, S. A. Diddams, J. Kitching, and M. T. Hummon, High-performance, compact optical standard, Opt. Lett. **46**, 4702 (2021).

[12] R. K. Raj, D. Bloch, J. J. Snyder, G. Camy, and M. Ducloy, High-frequency optically heterodyned saturation spectroscopy via resonant degenerate four-wave mixing, Phys. Rev. Lett. **44**, 1251 (1980).

[13] J. Ye, L. S. Ma, and J. L. Hall, Molecular iodine clock, Phys. Rev. Lett. **87**, 270801 (2001).

[14] K. Döringshoff, F. B. Gutsch, V. Schkolnik, C. Kürbis, M. Oswald, B. Pröbster, E. V. Kovalchuk, A. Bawamia, R. Smol, T. Schuldt *et al.*, Iodine frequency reference on a sounding rocket, Phys. Rev. Appl. **11**, 054068 (2019).

[15] J. Miao, T. Shi, J. Zhang, and J. Chen, Compact 459-nm Cs cell optical frequency standard with $2.1 \times 10^{-13}/\sqrt{\tau}$ short-term stability, Phys. Rev. Appl. **18**, 024034 (2022).

[16] H. Shang, T. Zhang, J. Miao, T. Shi, D. Pan, X. Zhao, Q. Wei, L. Yang, and J. Chen, Laser with 10^{-13} short-term instability for compact optically pumped cesium beam atomic clock, Opt. Express **28**, 6868 (2020).

[17] S. Lee, G. Moon, S. E. Park, H.-G. Hong, J. H. Lee, S. Seo, T. Y. Kwon, and S.-B. Lee, Laser frequency stabilization in the 10^{-14} range via optimized modulation transfer spectroscopy on the ^{87}Rb D_2 line, Opt. Lett. **48**, 1020 (2023).

[18] M. Hori, A. Sótér, D. Barna, A. Dax, R. Hayano, S. Friedreich, B. Juhász, T. Pask, E. Widmann, D. Horváth *et al.*, Two-photon laser spectroscopy of antiprotonic helium and the antiproton-to-electron mass ratio, Nature **475**, 484 (2011).

[19] F. Riehle, Optical clock networks, Nat. Photonics **11**, 25 (2017).

[20] C. Lisdat, G. Grosche, N. Quintin, C. Shi, S. M. F. Raupach, C. Grebing, D. Nicolodi, F. Stefani, A. Al-Masoudi, S. Dörscher *et al.*, A clock network for geodesy and fundamental science, Nat. Commun. **7**, 12443 (2016).

[21] S. Rothe, A. N. Andreyev, S. Antalic, A. Borschevsky, L. Capponi, T. E. Cocolios, H. De Witte, E. Eliav, D. V. Fedorov, V. N. Fedosseev *et al.*, Measurement of the first ionization potential of astatine by laser ionization spectroscopy, Nat. Commun. **4**, 1835 (2013).

[22] T. Schuldt, K. Döringshoff, E. V. Kovalchuk, A. Keetman, J. Pahl, A. Peters, and C. Braxmaier, Development of a compact optical absolute frequency reference for space with 10^{-15} instability, Appl. Opt. **56**, 1101 (2017).

[23] Z. Zhang, Z. Wang, H. Liu, W. Yuan, W. You, J. Zhang, K. Deng, and Z. Lu, An ultra-stable laser based on molecular iodine with a short-term instability of 3.3×10^{-15} for space based gravity missions, Class. Quantum Grav. **40**, 225001 (2023).

[24] Z. Liu, Z. Wang, X. Qin, X. Guan, H. Shi, S. Cao, S. Wei, J. Zhang, Z. Xiao, T. Shi *et al.*, Turn-key Voigt optical frequency standard, Photonics Res. **13**, 1083 (2025).

[25] P. Chang, S. Zhang, H. Shang, and J. Chen, Stabilizing diode laser to 1 Hz-level Allan deviation with atomic spectroscopy for Rb four-level active optical frequency standard, Appl. Phys. B **125**, 196 (2019).

[26] Z. Wang, Z. Liu, H. Shi, X. Qin, X. Guan, J. Zhang, Z. Gao, T. Shi, and J. Chen, Compact 852 nm Faraday optical frequency standard, Appl. Phys. Lett. **126**, 031103 (2025).

[27] H. Shang, D. Pan, X. Zhang, X. Xue, T. Shi, and J. Chen, Ultrastable laser referenced on velocity-grating atom interferometry, Phys. Rev. A **105**, L051101 (2022).

[28] W. G. Tobias, B. Hemingway, and S. Peil, Cold beam optical clock with multifrequency spectroscopy, Phys. Rev. Lett. **134**, 043401 (2025).

[29] E. Vicentini, A. Gambetta, N. Coluccelli, V. Di Sarno, P. Maddaloni, P. De Natale, A. Castrillo, L. Gianfrani, P. Laporta, and G. Galzerano, Absolute frequency stabilization of a QCL at 8.6 μm by modulation transfer spectroscopy, Opt. Lett. **45**, 4948 (2020).

[30] M. A. Gubin and E. D. Protsenko, Laser frequency standards based on saturated-dispersion lines of methane, Quantum. Elec. (Woodbury) **27**, 1048 (1997).

[31] M. K. Tarabrin, V. A. Lazarev, V. E. Karasik, A. N. Kireev, Y. V. Korostelin, A. S. Shelkovnikov, D. A. Tuyrikov, V. I. Kozlovsky, Y. P. Podmar'kov, M. P. Frolov, and M. A. Gubin, Application of the methane saturated dispersion resonance near 2.36 μm over the temperature range of 77–300 K for optical frequency standards, J. Quant. Spectrosc. Radiat. Transf. **177**, 241 (2016).

[32] P. T. Woods and B. W. Jolliffe, Stable single-frequency carbon dioxide lasers, J. Phys. E: Sci. Instrum. **9**, 395 (1976).

[33] E. Zang, J. Cao, Y. Li, C. Li, Y. Deng, and C. Gao, Realization of four-pass I_2 absorption cell in 532-nm optical frequency standard, IEEE Trans. Instrum. Meas. **56**, 673 (2007).

[34] L. Li, F. Liu, C. Wang, and L. Chen, Measurement and control of residual amplitude modulation in optical phase modulation, Rev. Sci. Instrum. **83**, 043111 (2012).

[35] W. Zhang, M. J. Martin, C. Benko, J. L. Hall, J. Ye, C. Hagemann, T. Legero, U. Sterr, F. Riehle, G. D. Cole *et al.*, Reduction of residual amplitude modulation to 1×10^{-6} for frequency modulation and laser stabilization, Opt. Lett. **39**, 1980 (2014).

[36] J. Zhang, X. Guan, X. Gao, Z. Wang, X. Qin, Z. Liu, H. Shi, J. Miao, T. Shi, and J. Chen, Power-stabilized 3-W blue laser locked to the 420-nm transition in rubidium, Phys. Rev. Appl. **22**, 034045 (2024).

[37] R. Wu, V. R. Supradeepa, C. M. Long, D. E. Leaird, and A. M. Weiner, Generation of very flat optical frequency combs from continuous-wave lasers using cascaded intensity and phase modulators driven by tailored radio frequency waveforms, Opt. Lett. **35**, 3234 (2010).

[38] Y. Dou, H. Zhang, and M. Yao, Generation of flat optical-frequency comb using cascaded intensity and phase modulators, IEEE Photonics Technol. Lett. **24**, 727 (2012).

[39] T. R. Schibli, I. Hartl, D. C. Yost, M. J. Martin, A. Marcinkevičius, M. E. Fermann, and J. Ye, Optical frequency comb with submillihertz linewidth and more than 10 W average power, Nat. Photonics **2**, 355 (2008).

[40] J. Grotti, S. Koller, S. Vogt, S. Häfner, U. Sterr, C. Lisdat, H. Denker, C. Voigt, L. Timmen, A. Rolland *et al.*, Geodesy and metrology with a transportable optical clock, Nat. Phys. **14**, 437 (2018).

[41] M. Takamoto, I. Ushijima, N. Ohmae, T. Yahagi, K. Kokado, H. Shinkai, and H. Katori, Test of general relativity by a pair of transportable optical lattice clocks, Nat. Photonics **14**, 411 (2020).

[42] R. M. Godun, P. B. R. Nisbet-Jones, J. M. Jones, S. A. King, L. A. M. Johnson, H. S. Margolis, K. Szymaniec, S. N. Lea, K. Bongs, and P. Gill, Frequency ratio of two optical clock transitions in $^{171}Yb^{+}$ and constraints on the time variation of fundamental constants, Phys. Rev. Lett. **113**, 210801 (2014).

[43] W. Ren, T. Li, Q. Qu, B. Wang, L. Li, D. Lü, W. Chen, and L. Liu, Development of a space cold atom clock, Natl. Sci. Rev. **7**, 1828 (2020).

[44] T. Bothwell, C. J. Kennedy, A. Aeppli, D. Kedar, J. M. Robinson, E. Oelker, A. Staron, and J. Ye, Resolving the gravitational redshift across a millimetre-scale atomic sample, Nature **602**, 420 (2022).

[45] S. Kolkowitz, I. Pikovski, N. Langellier, M. D. Lukin, R. L. Walsworth, and J. Ye, Gravitational wave detection with optical lattice atomic clocks, Phys. Rev. D **94**, 124043 (2016).